To cite this version :

Lucien LAIARINANDRASANA, Clémence DEVILLIERS, Sandrine. OBERTI, E GAUDICHET, Jean Marc LUCATELLI, Bruno FAYOLLE - Ring tests on high density polyethylene: Full investigation assisted by finite element modeling - International Journal of Pressure Vessels and Piping - Vol. 88, n°1, p.1-10 - 2011

Ring tests on high density polyethylene: Full investigation assisted by finite element modeling

L. Laiarinandrasana [a,*], C. Devilliers [a,b], S. Oberti [b], E. Gaudichet [b], B. Fayolle [c], J.M. Lucatelli [d]

[a] *MINES ParisTech, Centre des Matériaux, CNRS UMR 7633, BP 87, 91003 Evry Cedex, France*
[b] *Véolia Environnement, Centre de Recherche sur l'Eau, Chemin de la Digue, 78603 Maisons-Laffitte, France*
[c] *ARTS ET METIERS ParisTech, Laboratoire Ingénierie des Matériaux, UMR 8006, 151 boulevard de l'Hôpital, 75013 Paris, France*
[d] *CAE Caen, Laboratoire Matériaux, 40 avenue de la 1ère armée française, 14000 Caen, France*

ABSTRACT

In order to characterize the mechanical behavior of HDPE pipes, the ASTM D 2290-04 standard recommends carrying out tensile tests on notched rings, cut out from the pipe. This very simple test is also utilized to investigate the aging effect of the pipe by determining the strain at failure. Comparison between full ring and notched ring mechanical responses are discussed. Constitutive modeling including strain rate effects was performed by finite element analysis. This allowed a better understanding of the stress state in the cross section perpendicular to the loading direction. Additionally, the influence of a thin layer of oxidized HDPE in the inner wall of the ring was studied in the light of the finite element results.

1. Introduction

High Density PolyEthylene (HDPE) is a material widely used for the distribution of drinking water. Pipes are subjected to an internal pressure due to water flow. Furthermore, when they are in contact with disinfectants such as chlorine dioxide ClO$_2$, oxidation of HDPE occurs by a chain scission phenomenon. Oxidation turns out to be highly confined to the immediate surface of the inner wall in contact with ClO$_2$, leading to a decrease of molar mass and a multicrack network. A gradient of degradation can be considered. The oxidation profile shows a maximum value at the internal wall [1]. In order to classify the degradation of HDPE pipes, Rozental-Evesque et al. [2] carried out Nol ring tests and used the strain at failure as a key parameter.

Historically, the ring expanding test was first recommended by International Standard ISO 8495-8496 [3] for characterizing thin metallic material tube. The main purpose was then to measure the transverse properties of structural tubing. Available exact solutions of the stress distribution in the cross section of the tube were proposed by Bagci [4,5] for isotropic linear elastic behavior of the material. In particular, it was reported that there exists a bending effect in the horizontal cross section, due to the loss of roundness of the ring during the loading. In order to prevent this bending effect, Arsène and Bai [6,7] proposed a new approach by adapting the experimental setup, for a material exhibiting non-linearity (plasticity) in its mechanical behavior.

Reference [2] followed the recommendation of ASTM D 2290-04 standard [8] dealing with the characterization of the "*apparent hoop tensile strength*" of plastic material for structural tubing. To this end, tensile tests have to be performed on rings, cut out from the pipe, by a split disk method. The specimen is loaded through two half cylinders, which apply tensile stress to the ring. The term "*apparent*" here deals with the heterogeneity of the stress in the cross section of the ring, due to the bending effect already reported by Arsène and Bai [6]. To overcome this difficulty, it is suggested to use notched ring specimens. However, for Zircaloy cladding [6,7], putting notches in the ring did not eliminate this bending effect. Furthermore, a defect such as a notch in a structure enhances both heterogeneity and the multiaxial state of the stress in the cross section. The first goal of this paper is then to compare data on rings with and without notches.

The HDPE material exhibits non-linear behavior (plasticity) as well as time dependent deformation even at room temperature. These non-linearities interfere with the complex stress state within the material when running a Nol ring test. In this work, finite element (FE) analysis was extensively used to account for non-linearity and multiaxial stress state with the help of an efficient constitutive modeling.

The first section of the article presents the material under study, followed by the experimental procedures applied to various specimens. The experimental results in terms of stiffness, maximum stress and strain at failure are detailed and discussed in Section 3. In Section 4, FE modeling is described. The true stress—strain curves are derived from an inverse method optimization. In the light of the computation results, discussions are carried out about the local stress state as well as the effect of a thin layer of degraded material in the inner wall of the ring.

2. Experimental procedure

2.1. Material and specimens

The main physico-chemical characteristics of the HDPE studied are summarized in Table 1. The crystallinity index X_c and the melting point T_f were determined by using Differential Spectroscopy Calorimetry (DSC). Gel Permeation Chromatography (GPC) allowed the measurement of various molar masses, such as the number average molar mass (M_n), the weight average molar mass (M_w) and the Z average molar mass (M_z). The fillers' content investigations were performed with thermo-gravimetric analysis, yielding that there is 2.2% of carbon black and a negligible amount of other chemical species (for instance, catalytic residues). It is to be mentioned that the glass transition temperature T_g of HDPE is a controversial subject. Indeed, in the Polymer Handbook [9], it is reported concerning the HDPE that: "*Considerable disagreement exists between authors on the exact value of the transition which can be identified as the glass transition temperature*". Namely, three distinct values of T_g were found: -30 ± 15 °C, -80 ± 10 °C and -128 ± 5 °C according to Refs. [10–14]. However, in this work, the testing temperature (room temperature) is considered to be well above the glass transition temperature (T_g) of the HDPE.

For this specific study, several pipes were supplied (Fig. 1a), whose dimensions are: length = 500 mm; internal diameter $\phi_0 = 31$ mm, and thickness $t = 4.5$ mm. From these pipes, two types of specimen were machined:

- small dog-bone shaped specimens taken from the circumferential direction in order to measure the transverse stress—strain curve. The representative volume element dimensions were: section = (2 mm × 1.4 mm), gauge length = 6 mm.
- ring specimens (width, $W = 12$ mm), composed of: i) full ring (Fig. 1b) and ii) notched ring (Fig. 2).

2.2. Experimental procedure

The test programme was carried out in two laboratories in order to check the repeatability (within the same laboratory) and the reproducibility (with two different laboratories) of the results. At CAE Caen, a testing machine with a load capacity of 10 kN was used whereas at ENSAM ParisTech (referred to as LIM), ring and dog-bone tests were performed on a machine with a load cell capacity of 10 kN and a machine with a load capacity of 1 kN. In all cases, the crosshead displacement was measured during the test. Some tests were provided with video camera for observations purposes at critical events of the tensile tests.

**Table 1**
Physico-chemical characteristics of HDPE.

Parameters	X_c	T_f	M_n	M_w	M_z
Values	55%	127 °C	10.2 kg/mol	206.5 kg/mol	2343.25 kg/mol
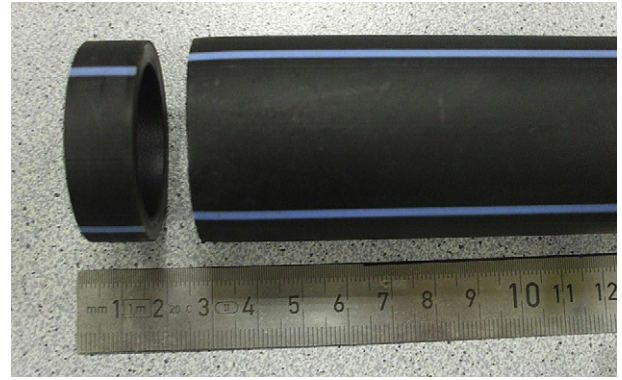
**Fig. 1.** HDPE material supply: full Nol ring specimen (slice of $W = 12$ mm wide of the pipe). Nominal section is 4.5 mm × 12 mm = 54 mm² extracted from a pipe of 500 mm, thickness $t = 4.5$ mm, internal diameter $\phi_0 = 31$ mm.

The first tests were performed with the fixture device proposed by ASTM D 2290-04 [8] (see Fig. 3a,b). With this system, preliminary results on full rings showed half disk rotation inducing asynchronous necking in both sides of the ring (see Fig. 3b). Indeed, the first necking systematically appeared in the more elongated side of the ring, presumably due to the contact with the sharp edge of the rotated half disk. This phenomenon impairs the axisymmetry of the specimen during the last part of the loading. In order to prevent this rotation, half disks were fixed and their sharp ends were smoothed (blunted) in the new fixture setup (Fig. 3c). Note that, notches implanted in the rings were expected to reduce these effects.

The test programme, summarized in Table 2, aimed to analyze the effects of:
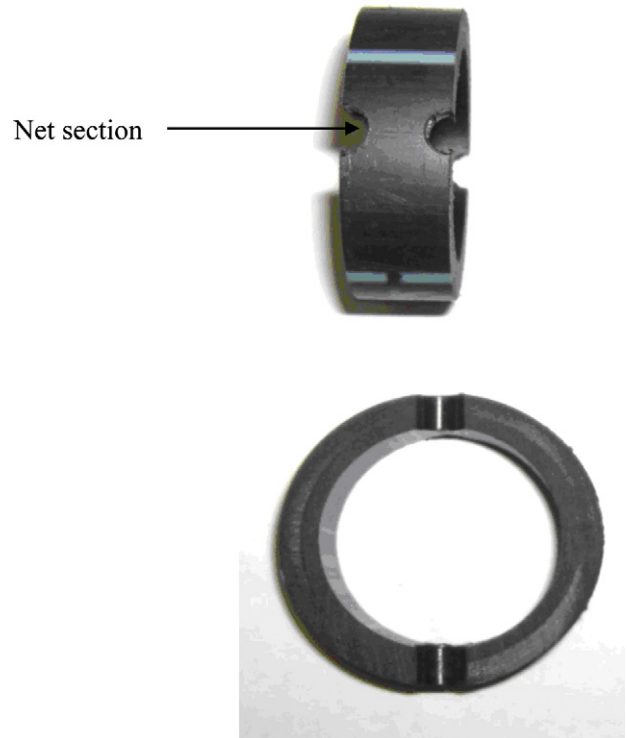
Fig. 2. Notched Nol ring specimen: notch radius $\rho = 3$ mm obtained by "drilling". Net section is 4.5 mm × 6 mm = 27 mm².
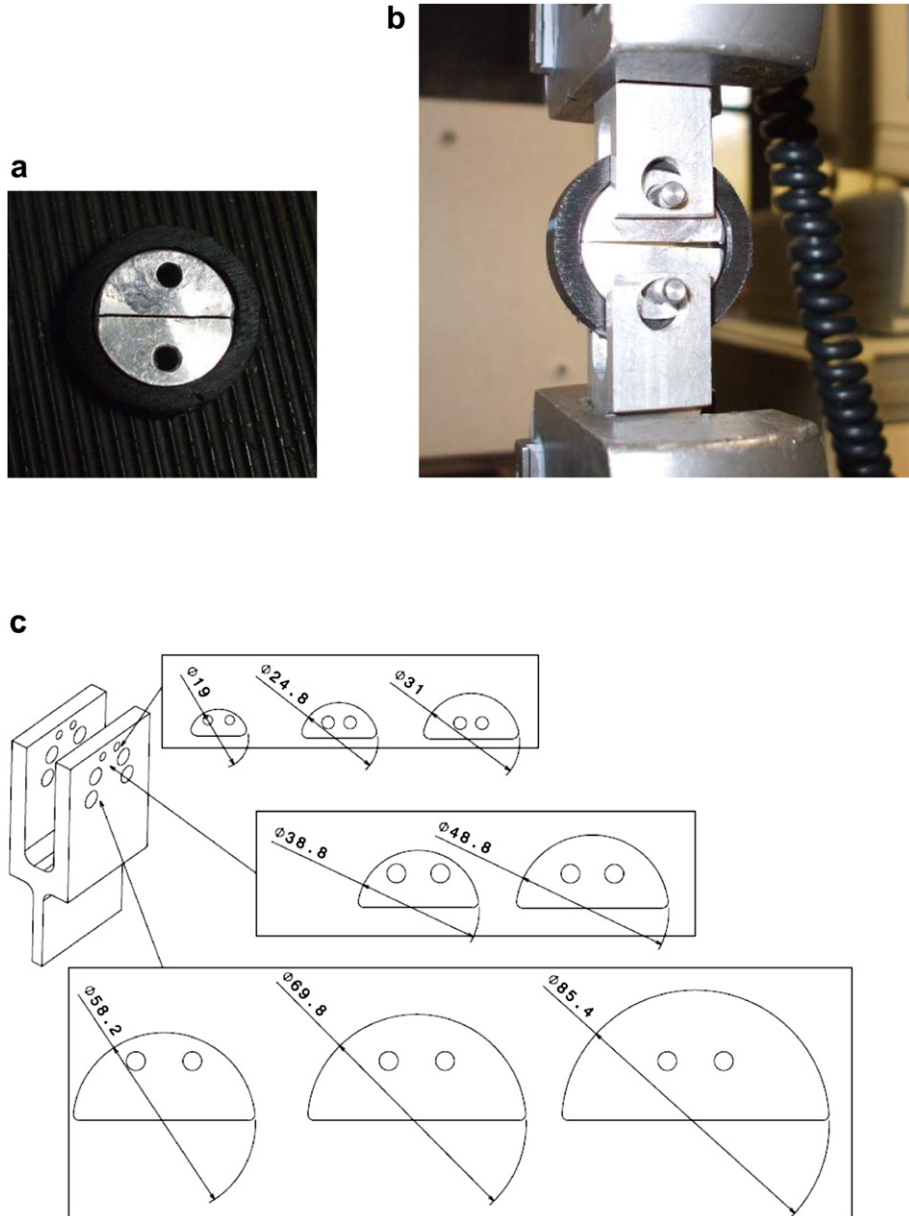
Fig. 3. Nol ring fixtures on the traction machine load-line: a) half disks with full ring; b) rotation of half disks, clearance in the right side of the ring is bigger than that of the left side; c) new fixture system for various ring diameters: fixation and smoothing of the sharp ends of half disks (*dimensions in mm*).

- full ring versus notched ring mechanical responses;
- crosshead speed (10 mm/mn; 50 mm/mn and 100 mm/mn);
- uniaxial (small dog-bone and maybe full ring) versus multi-axial (notched ring) stress states.

3. Experimental results

The total numbers of tests are shown in boldface in Table 2. As mentioned earlier, all tests were multiplied in order to have an idea

Table 2
Tests programme at room temperature for various specimen geometries of PEHD material.

Crosshead speeds	10 mm/mn	50 mm/mn	100 mm/mn
	Total (LIM + CAE)	Total (LIM + CAE)	Total (LIM + CAE)
Full ring (FR)	18 (8 + 10)	10 (5 + 5)	10 (5 + 5)
Notched ring (NR)	15 (10 + 5)	5 (5 + 0)	9 (5 + 4)

of repeatability (scatter within the same laboratory results) as well as reproducibility (comparison between the two laboratories results).

First, it has to be mentioned that in the early stage of the load versus displacement curve for ring tests, a non-linear part appears (Fig. 4). Since there is a clearance of 1 mm between the outer diameter of the half disks and the inner diameter of the ring specimens, the non-linear part is due to the gradual contact between both faces. The end of this step is reached when the load versus displacement curve becomes linear. The first non-linear part was systematically neglected, by shifting the load-displacement curve based on the extension of the linear part to the displacement axis (see vertical arrow in Fig. 4).

3.1. Consecutive necking phenomena in full ring

Figure 5a displays representative engineering stress−strain curves at three different crosshead speeds of full rings (Fig. 1b): the
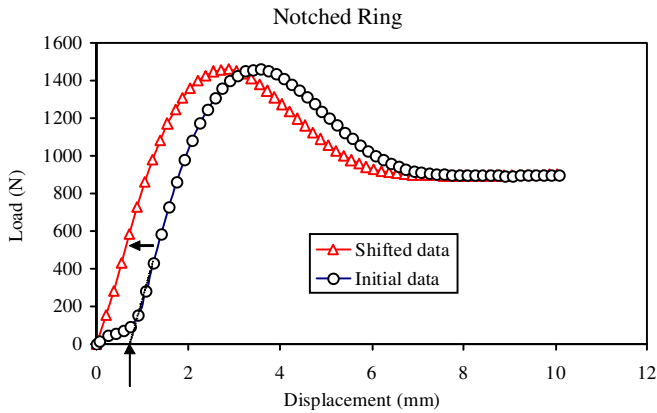
Fig. 4. Load versus applied displacement curve for notched ring at 100 mm/mn crosshead speed. Curve shifted to the left in order to avoid the effect of clearance reduction in the beginning of the test. This allows estimating the stiffness.

engineering stress and strain being F/S_0 where F is the load and S_0 is twice the initial cross section of the ring ($S_0 = 12$ mm $\times$ 4 mm $\times$ 2); and $\Delta\phi/\phi_0$ where $\Delta\phi$ is the diametrical variation applied by the crosshead and $\phi_0 = 31$ mm is the initial diameter. These curves were plotted until the total failure of the ring specimen. Thanks to the video camera, critical events during the test could be associated to the stress—strain curves shape. These curves exhibit maximum stresses where generally necking on one side of the ring appears
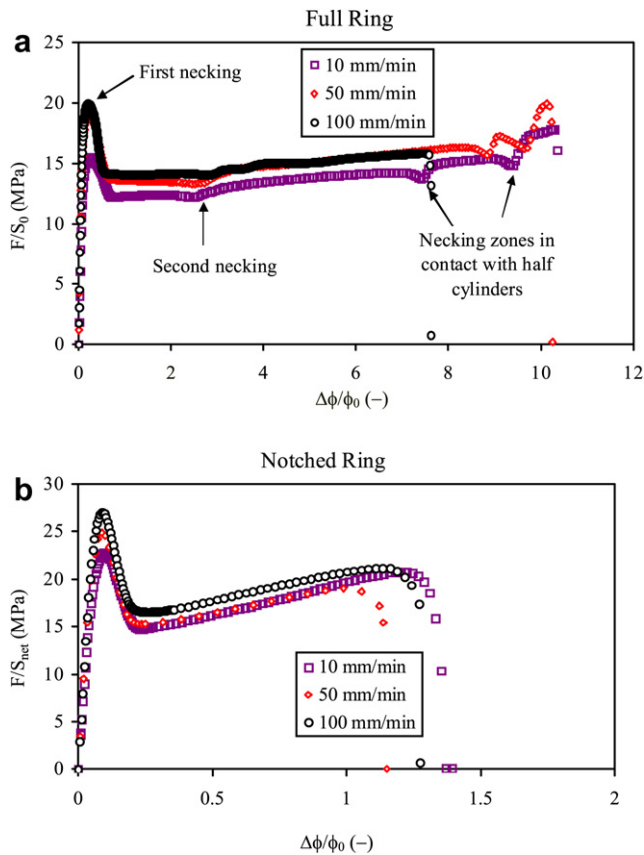
Fig. 5. Effect of crosshead speed on stress—strain complete curves. a) full ring: engineering stress (F/S_0) versus engineering strain ($\Delta\phi/\phi_0$) with $S_0 = 12 \times 4.5 \times 2 = 108$ mm^2 and $\phi_0 = 31$ mm; b) notched ring: net stress (F/S_{net}) versus engineering strain ($\Delta\phi/\phi_0$) with $S_{net} = 6 \times 4.5 \times 2 = 54$ mm^2 and $\phi_0 = 31$ mm.

although the half disks were fixed. A second event, represented by a discontinuity, occurs in all curves at an engineering strain of about 2.7, shown by the arrow in Fig. 5a. Here, necking appears on the other side of the ring. This is likely due to the alignment defect of half cylinders (not constant clearance between both) as well as defect distributions in the material under study. Further "discontinuities" appear when the necking zone reaches contact with the cylinder outer diameter. This may happen simultaneously (for instance the test at 100 mm/mn) or separated in time (for both 10 mm/mn and 50 mm/mn). The end of the test corresponded to specimen failure. It can be concluded that avoiding half disk rotation does not prevent asynchronous necking in both sides of the ring. However, it seems that the second necking happens at approximately the same strain regardless of the crosshead speed.

3.2. Effects of specimen geometry (full versus notched rings)

Similar to the full rings (Fig. 5a), Fig. 5b plots the engineering stress—strain curves of notched rings. Since the notches reduce the section of the investigated volume, the engineering stress definition was changed to net stress which is equal to F/S_{net}, where F is the load and S_{net} is twice the net section of the specimen (see Fig. 2), that is $S_{net} = 6$ mm $\times$ 4 mm $\times$ 2. The definition of the engineering strain is the same as in Section 3.1. Curves are rather smooth, without any discontinuity after the maximum stress. So, notches in the ring specimens seem to be interesting, at least for global parameter relationships such as engineering stress—strain curves. Indeed, notches tend to localize deformation in the net section. Therefore, first necking occurs in both sides of the ring test. It is to be noticed that the drop of the stress following the maximum stress is twice as much in the notched ring as in the full ring. This indicates that synchronous necking took place. By examining the shapes of the stress—strain curves in Fig. 3 of Ref. [3], one can notice that, on notched rings, there exist two discontinuities. Recalling that the half disks were not fixed in these tests, it can be guessed that necking was asynchronous but the extended necked zones reached the half disks at approximately the same time. One can conclude that discontinuities disappear for fixed disks and notched ring specimens.

However, it is well known [15] that the presence of notches induces, in the net section, stress heterogeneity (gradient) and stress multiaxiality. Indeed, it is observed that strain and stress values on full rings, respectively, are lower and higher on notched rings. This effect is due to the stress triaxiality ratio [15] set by the notches in the net section.

3.3. Results for stiffness, maximum stress, ductility

In this section, some key parameters are discussed. For the sake of clarity, tables and figures are given. In the figures, full symbols deal with LIM data whereas open symbols are for those of CAE. In addition, dashed lines represent the scatter boundaries of the experimental results according to the origin of the data (LIM or CAE). Note also that there is no available data at CAE, for notched rings at 50 mm/mn crosshead speed.

3.3.1. Stiffness
The stress in the cross section of the ring is not homogeneous (bending effect). The slope in the linear part at the beginning of the stress—strain curve will be called the stiffness instead of the Young's modulus. Here, stiffness is defined as the engineering stress (F/S_0) for the full ring and net stress (F/S_{net}) for the notched ring respectively, divided by the engineering strain $\Delta\phi/\phi_0$. Table 3 and Fig. 6a detail the experimental results for the stiffness values, plotted against the crosshead speeds (10 mm/mn, 50 mm/mn and 100 mm/mn).

Table 3
Full ring and notched ring results on stiffness (in MPa).

Crosshead speeds		10 mm/mn	50 mm/mn	100 mm/mn
Full ring	LIM	109.0 ± 7.2	132.0 ± 5.9	148.4 ± 6.3
	CAE	124.4 ± 9.2	148.7 ± 14.0	162.0 ± 12.8
	Total	116.7 ± 18.2	140.3 ± 18.3	155.2 ± 16.3
Notched ring	LIM	217.6 ± 11.8	237.2 ± 12.3	255.9 ± 6.2
	CAE	237.3 ± 7.1		315.5 ± 33.2
	Total	227.4 ± 19.3	237.2 ± 12.3	285.7 ± 49.5

Starting with the full ring results, located in the lower part of Fig. 6a, LIM values (full symbols) are systematically lower than those of CAE (open symbols). The lower limit of the scatter band of the CAE data interferes with that of LIM. Repeatability is good, in particular for LIM data and reproducibility is rather poor. It is observed that the higher the crosshead speed, the higher the stiffness value. This expected result is clearly shown in Fig. 6a as well as in Table 3 which lists the average values.

Stiffness for the notched ring is a factor 2 higher than that of the full ring. This is only due to the cross section of the notched ring being a factor 2 lower than that of the full ring. The scatter band for CAE notched ring data is as large as that of full ring, whereas for LIM data, the full ring has better repeatability (narrower scatter band) compared with the notched ring data.

The stiffness parameter seems to follow the expected trend from a mechanical properties viewpoint. Repeatability is good demonstrating the relevance of such a parameter. Reproducibility problem

Fig. 6. Main experimental results a) Stiffness; b) Maximum stress.

needs further investigations whereas later mechanical response investigations will be based on LIM data.

3.3.2. Maximum stress

Table 4 and Fig. 6b illustrate experimental values for the maximum stress, *i.e.* at the onset of first necking. According to the ring geometry, the stresses have different definitions here: nominal stress and net stress for the full and notched ring, respectively. Figure 6b clearly shows that the higher the crosshead speed, the higher the maximum stress whatever the data origin. Similarly to the stiffness, this trend was expected, as the material exhibited strain rate effects. It can be observed that full ring data are located in the lower part of the diagram, presumably due to the stress definition and the triaxiality effect as mentioned previously. The results on full ring tests show excellent agreement between the two laboratories. Repeatability and reproducibility were satisfactory, and confidence in the mean values of maximum stresses in Table 4 is high.

For notched rings data, it can be observed that CAE values are generally higher than those of LIM. Repeatability is good for CAE whereas it is acceptable for LIM. These latter data show that the higher the crosshead speed, the more scattered the experimental points. It can then be concluded that average values of maximum stress must be taken within each laboratory data. Although mean values are given for notched rings in Table 4, it is not convenient to use them.
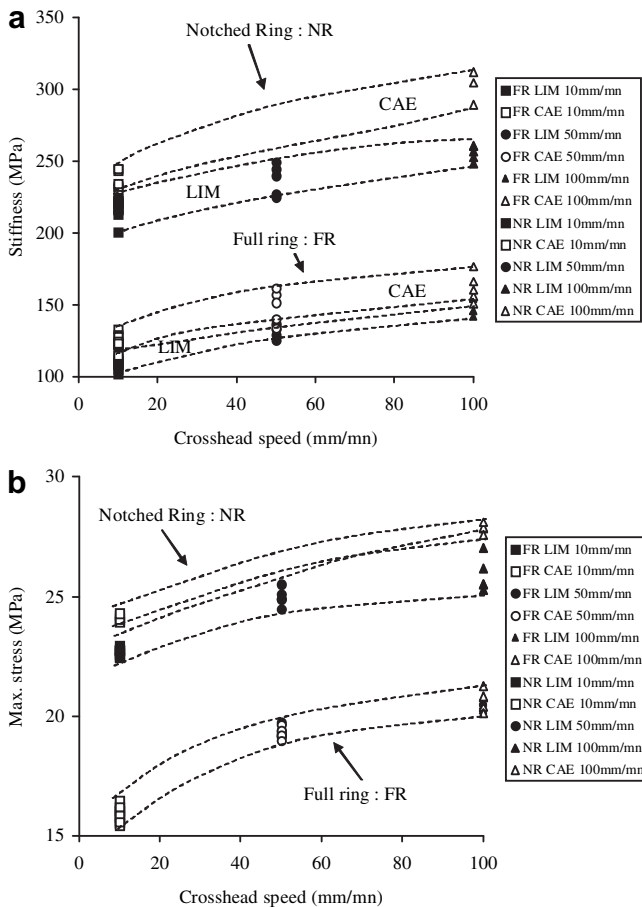
The maximum stress is then an interesting parameter, useful for mechanical properties characterization.

3.3.3. Ductility or strain at failure

The definition of strain is the same in both geometries. However, the triaxial stress state in the cross section of notched rings induces lower strain values. Additionally, strain at failure is subjected to experimental artefacts, as previously mentioned. Consecutive necking that cannot have the same number for two different tests impair repeatability as well as reproducibility of the ductility. Table 5 summarizes ductility values that are plotted in Fig. 7. In Fig. 7a illustrating the ductility obtained on full ring specimens, it can be observed that the values of strain are very high ($\Delta\phi/\phi_0 > 10$). This is due to the definition of the gage length (here the inner diameter $\phi_0 = 31$ mm) whereas large extension of the necks is observed. Although, LIM data (full symbols) indicate a normal evolution of the ductility with respect to the crosshead speed, the scatter bands are so large that it is inappropriate to use Fig. 7 data. Therefore, it is not recommended to use the ductility obtained from the Nol ring test to assess aging effects on tubes.

3.4. "Intrinsic" curves

In Subsection 3.3 an attempt was made to analyze all parameters that can be extracted from stress−strain curves (Fig. 5). It was mentioned that parameters obtained before the first necking (stiffness and maximum stress) are the most relevant, regarding the effect of crosshead speed. Indeed, necking can be considered as

Table 4
Full ring and notched ring results on maximum stress (in MPa).

Crosshead speeds		10 mm/mn	50 mm/mn	100 mm/mn
Full ring	LIM	16.0 ± 0.4	19.3 ± 0.3	20.4 ± 0.2
	CAE	15.7 ± 0.8	19.3 ± 0.3	20.7 ± 0.6
	Total	15.9 ± 0.8	19.3 ± 0.3	20.6 ± 0.6
Notched ring	LIM	22.7.0 ± 0.2	25.0 ± 0.5	25.9 ± 0.9
	CAE	24.1 ± 0.2		27.9 ± 0.3
	Total	23.4 ± 0.9	25.0 ± 0.5	26.9 ± 1.6

Table 5
Full ring and notched ring results on ductility.

Crosshead speeds		10 mm/mn	50 mm/mn	100 mm/mn
Full ring	LIM	11.3 ± 1.5	9.1 ± 3.8	8.6 ± 3.5
	CAE	26.6 ± 1.4	20.3 ± 12.9	14.9 ± 12.6
	Total	18.9 ± 9.1	14.7 ± 13.9	11.7 ± 11.2
Notched ring	LIM	1.1 ± 0.3	1.2 ± 0.1	1.0 ± 0.2
	CAE	2.5 ± 0.9		1.9 ± 0.3
	Total	1.8 ± 1.3	1.2 ± 0.1	1.4 ± 0.7

a geometrical defect, therefore, the initial representative volume element is no longer homogeneous as soon as the necking appears.

On the other hand, it was mentioned that a bending effect is expected to occur in the horizontal cross section of the ring. The engineering stress−strain curve cannot describe this stress state. Intrinsic (true) stress−strain curves have to be investigated instead. To this end, the first part of the stress−strain curves from LIM data (Fig. 5), up to the maximum stress are plotted in Fig. 8. These curves do not suffer from experimental artefacts, but they still remain "global" in the sense that they cannot fully reflect transverse material properties at the horizontal cross section. Two investigations are proposed in the following. The first one deals with extraction of mini dog-bone specimens from the tubes. Tensile tests at 10 mm/mn and 100 mm/mn were carried out on these small specimens (gage length 6 mm, width 2 mm, thickness 1.4 mm).
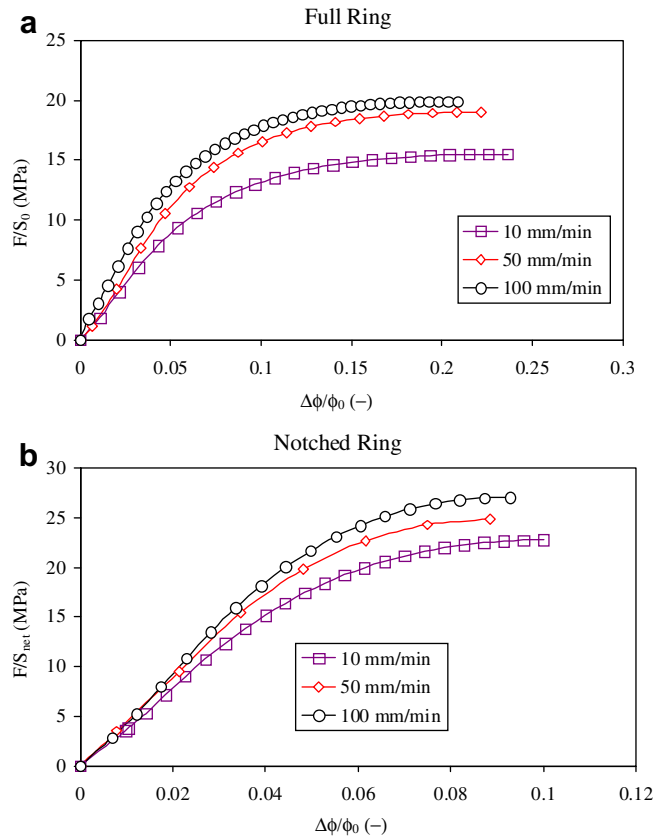
Fig. 8. Effect of crosshead speed on stress−strain curves up to maximum stress. a) full ring: engineering stress (F/S_0) versus engineering strain ($\Delta\phi/\phi_0$) with $S_0 = 12 \times 4.5 \times 2 = 108$ mm^2 and $\phi_0 = 31$ mm; b) notched ring: net stress (F/S_{net}) versus engineering strain ($\Delta\phi/\phi_0$) with $S_{net} = 6 \times 4.5 \times 2 = 54$ mm^2 and $\phi_0 = 31$ mm.

Additional experimental results are shown in Fig. 9. Figure 9b focuses on stress−strain curves up to the maximum stress. The HDPE Young's modulus E was graphically estimated from these stress−strain curves. Namely $E = 600$ MPa. Only experimental points (symbols with lines) are discussed here. It can be observed that the maximum stresses are ordered as follows: full ring < notched ring < small dog-bone. This demonstrates, at this scale, the effect of bending stress such that: full ring > notched ring > small dog-bone. Using notched ring tends to reduce the bending effect but cannot eliminate it.

The second approach is based on the use of FE code, which requires constitutive modeling dealing with the intrinsic (true) stress−strain curve of the material. In order to optimize material parameters, the use of an inverse method is necessary. Investigations in this way should be carried out with the help of the experimental data in Figs. 8 and 9b. Typically, effects due to the crosshead speed and the geometry (full ring, notched ring, small dog-bone specimen) have to be accounted for when addressing the modeling of the mechanical behavior via the FE method. This allows then accessing the distribution of stress/strain in the horizontal cross section.

4. Finite element modeling

In this section, an in house FE code [16] was used. This code is provided with an optimizer routine [17] that allows determination of the set of material parameters, related to an already implemented constitutive model.
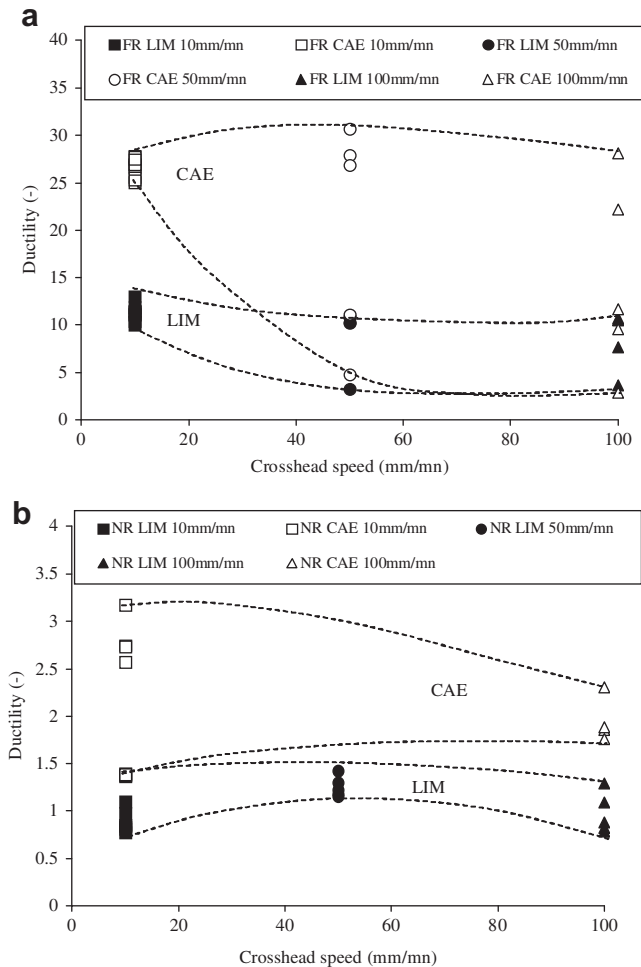
Fig. 7. Ductility a) Full ring; b) Notched ring.
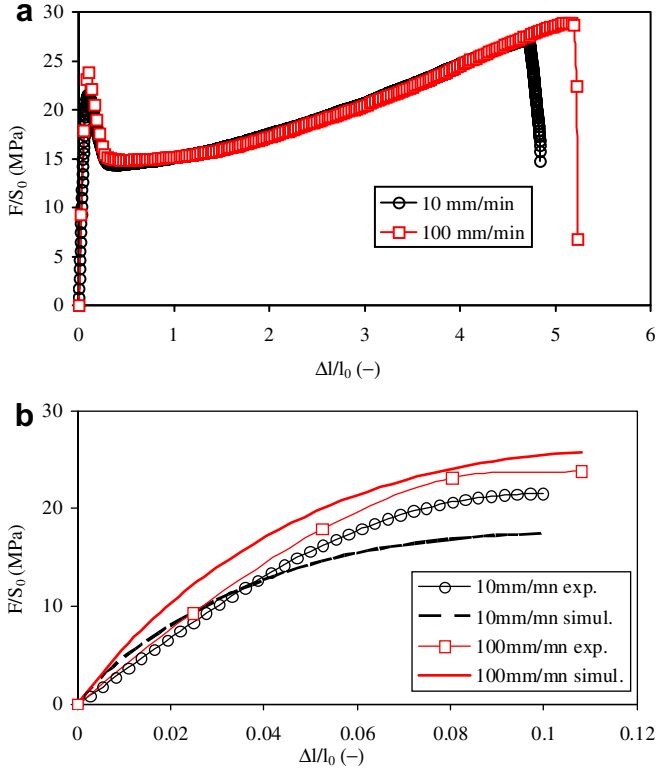
Fig. 9. Engineering stress F/S_0 versus engineering strain $\Delta l/l_0$ curves at two crosshead speeds for small dog-bone specimens a) until failure; b) stopped at maximum stress.

4.1. FE computation description

4.1.1. Meshes

Although full ring can be studied in 2D (generally under plane stress conditions), it is necessary to use 3D meshing for the notched ring. In order to avoid extra discussion about plane stress versus plane strain hypotheses, we focus here on 3D meshes (Fig. 10). Figure 10a shows 3D meshing of 1/8 of the full ring constituted of 1482 quadratic brick elements and 24025 degrees of freedom. For the notched ring (Fig. 10b), refined meshes in the vicinity of the notch were necessary. Therefore, 4632 quadratic brick elements were used, with 67170 degrees of freedom. The notched ring is then significantly more time consuming in terms of numerical modeling.

The small dog-bone specimen data were modeled by using a Representative Volume Element (RVE), provided in the FE code.

4.1.2. Constitutive equation

In order to take all the deformation components into account, a classical elastic−viscoplastic model is proposed [18,19] and described as follows.
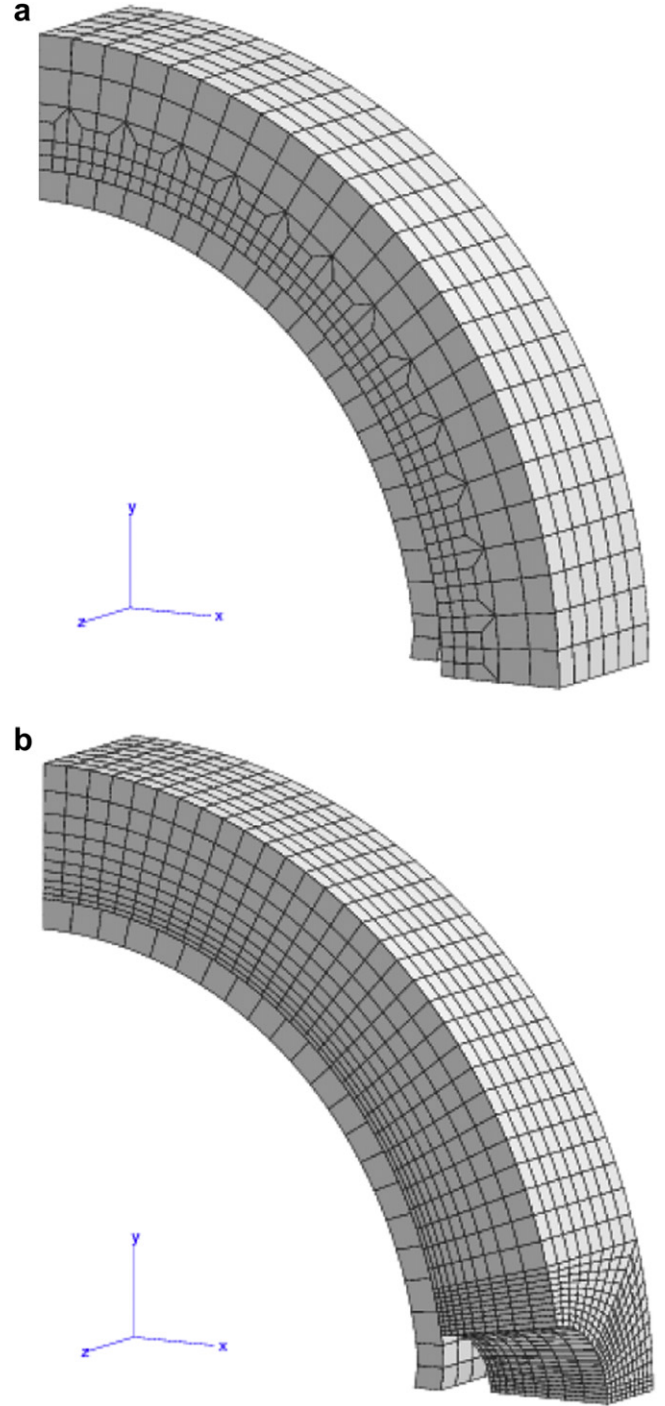
The plastic flow potential Φ is written as

$$\Phi = J\left(\tilde{\sigma} - \tilde{X}\right) - R(p) \tag{1}$$

where $\tilde{\sigma}$ is the stress tensor and $J(\tilde{\sigma})$ is the von Mises plasticity criterion; p is the accumulated plastic strain representative of the material hardening; $\tilde{X}$ is the back stress tensor whose evolution laws are written as follows:

$$\tilde{X} = \frac{2}{3}C\tilde{\alpha} \tag{2}$$

$$\tilde{\alpha} = \dot{p}\left(\frac{\partial \Phi}{\partial \tilde{\sigma}} - \frac{3D}{2C}\tilde{X}\right) \tag{3}$$

Fig. 10. 3D meshing of 1/8 ring specimens a) full ring; b) notched ring.

R is the yield stress of the material that follows the plastic hardening:

$$R(p) = R_0 + Q\left(1 - e^{-bp}\right) \tag{4}$$

In order to take strain rate effects into account, a Norton flow law is used:

$$\dot{p} = \dot{p}_0\left\langle\frac{\phi}{K}\right\rangle^n \tag{5}$$

where $\dot{p}_0$ is fixed to 1 s^{-1}.

In Eqs. (1–5), material coefficients are R_0, Q, b, C, D, K and n. The values of these material parameters are summarized in Table 6 corresponding to the line entitled "Virgin" HDPE.

4.1.3. Boundary conditions

In Fig. 10, typical meshes are shown and by symmetry the boundary conditions consist of:

- y-axis displacement blocked on plane $x = 0$ (horizontal cross section);
- x-axis displacement blocked on plane $y = 0$ (vertical cross section);
- z-axis displacement blocked on plane corresponding to half width of the specimen.

The upper part of the half cylinder is represented by the internal ring constituted by rigid elements. Contact is ensured at the interface between the rigid surface and HDPE, with a friction coefficient of 0.2. In this work, there was no sensitivity study of the results regarding this parameter.

The displacement is imposed on the rigid body, following the y-direction and according to the investigated crosshead speed.

4.2. Results in terms of global response (nominal stress/strain curve) up to ultimate strength

By using the same set of material coefficients in the FE simulations, engineering stress–strain curves were plotted in Fig. 11a for full ring and Fig. 11b for notched ring. Additionally, the comparison between experimental and simulated value for dog-bone specimen is illustrated in Fig. 9b (lines). It can be observed that all simulated curves are in good agreement with the experimental ones. Namely, the effects of crosshead speed are very well matched. Furthermore the ratio between engineering strains for full ring versus notched ring (factor 10) obtained experimentally is reproduced by the calculation. Thus, specimen geometry effects as well as strain rate effects are accounted for by the FE analysis. At this stage, one can argue that by optimizing material coefficients with the inverse method assisted by the FE code on one of the two geometries—say full or notched ring—one can "produce" complementary data for the other geometry. Furthermore, the agreement obtained in Fig. 11 allows "local" analyses of the stress state.

4.3. Local stress/strain fields: bending effects

The study of the mechanical properties of a given material is based on a stress–strain curve issued from a representative volume element (RVE). Within this RVE, the stress is both homogeneous and uniaxial. In the following, the stress and stress tensors at the horizontal cross section of rings are obtained from FE analysis. According to Bagci [4,5], there are no shearing stresses in this section, perpendicular to the loading direction. The discussions are then focused on σ_{yy} (hoop stress, in the direction of tension), σ_{xx} (radial stress, in the direction of the thickness) and σ_{zz} (longitudinal stress, in the direction of the width). Typically, in the prescribed cross section, in order to fulfill the abovementioned RVE conditions, σ_{yy} should be constant in the whole section and $\sigma_{zz} = \sigma_{xx} = 0$. The

Table 6
Values of the material coefficients for HDPE under study.

| Parameters	E (MPa)	ν	Q (MPa)	b	C (MPa)	D	n	K (MPa)
"Virgin" HDPE	600	0.4	12	48	201	145	2.2	46
Oxidized HDPE	1076	0.4	8.7	85.7	370	172.6	6.1	39.9

$R_0 = 0$ for both materials.
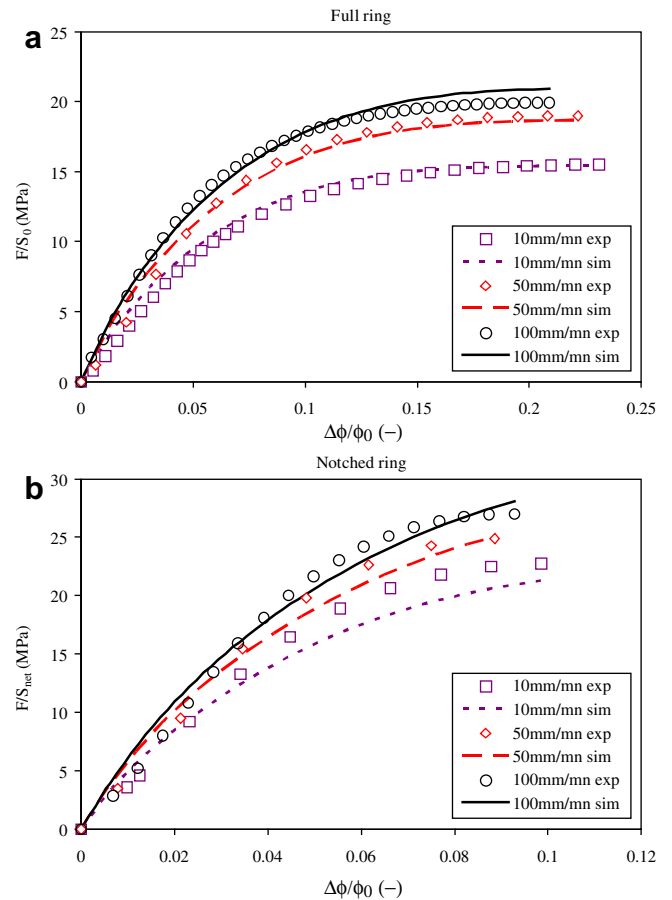
Fig. 11. Comparison between experimental ("exp" symbols) and simulated ("sim" lines) curves at various crosshead speeds. a) Full ring; b) Notched ring.

following comments are made on the simulations of ring tests at 100 mm/mn crosshead speed and when the maximum stress is attained. Therefore, the diagrams display σ_{xx}, σ_{yy}, σ_{zz}, respectively normalized by either the maximum nominal stress (σ_{nom}^{max}), for full rings, or the maximum net stress (σ_{net}^{max}) in the case of notched rings, with respect to the relative position in the width and in the thickness. In this kind of illustration, homogeneous and uniaxial stress is represented by a plane $\sigma_{yy}/\sigma_{nom}^{max} \approx 1$ alone, σ_{xx} and σ_{zz} being null.

4.3.1. Full ring

Figure 12 displays in 3D the distribution of all stress tensor components, in the horizontal cross section, with respect to both the relative location through the thickness and the whole width. The stress is normalized by the maximum stress (here $\sigma_{nom}^{max} = 20$ MPa). Figure 12a clearly shows that σ_{yy} is not homogeneous: a bending effect exists. In the internal diameter of the full ring, the axial σ_{yy} stress is higher than the applied stress whereas in the outer diameter, compressive σ_{yy} stress is observed. Through the thickness, $\sigma_{yy}/\sigma_{nom}^{max}$ values range from -0.4 to 1.5, yielding $\sigma_{yy} \approx 2\sigma_{nom}^{max}$. Through the width of the ring, it seems that σ_{yy} is quite constant with a slight deviation near to the faces.

σ_{zz} distribution is depicted in Fig. 12b whereas σ_{xx} is negligible. It appears that σ_{zz} also is not homogeneous. Both figures show that the stress state is neither homogeneous (σ_{yy} gradient) nor uniaxial ($\sigma_{zz} \neq 0$). That is why FE analysis is required for the ring test, even if the geometry is not notched. Additionally, in order to reduce time consumption for full rings, 2D computation can be run with plane strain conditions, due to $\sigma_{zz} \neq 0$.
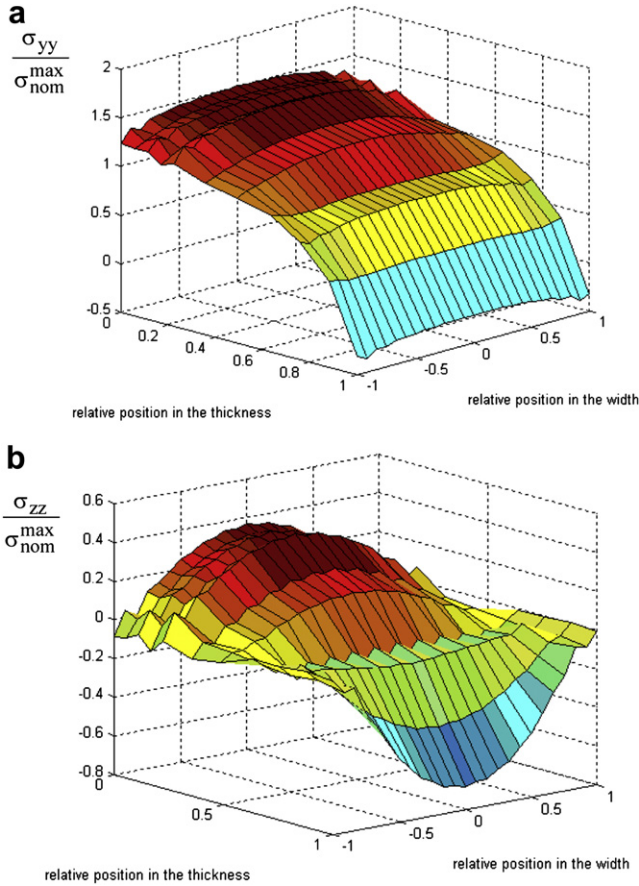
Fig. 12. Full ring: 3D representation of the stresses distribution in the cross section at maximum stress $\sigma_{nom}^{max} = 20$ MPa for 100 mm/mn crosshead speed. a) normalized hoop stress $\sigma_{yy}/\sigma_{nom}^{max}$; b) normalized longitudinal stress $\sigma_{zz}/\sigma_{nom}^{max}$.
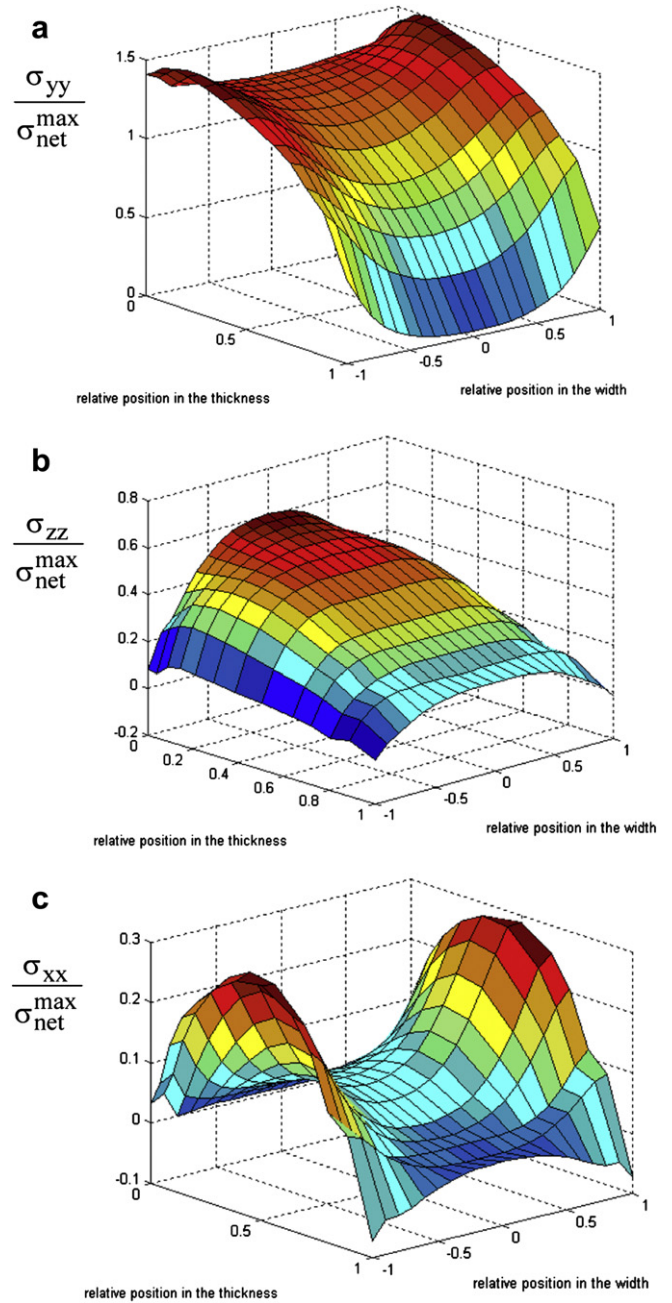
4.3.2. Notched ring

Figure 13 shows the same features for the notched ring ($\sigma_{net}^{max} = 27$ MPa). In particular, Fig. 13a clearly shows that although the bending effect is still present (σ_{yy} gradient through the thickness), the outer diameter of the ring does not experience compressive stress. The σ_{yy} gradient is lower compared to that of the full ring. Indeed, here, along the thickness abscissa, $\sigma_{yy}/\sigma_{net}^{max}$ values range from 0.1 to 1.4. Thus, $\Delta\sigma_{yy} \approx 1.5\,\sigma_{net}^{max}$. In the width direction, the notch gives a stress concentration in the vicinity of the notch root. Figure 13b,c show that both σ_{xx} and σ_{zz} are not negligible and have their own distributions (not homogeneous). The notched ring has higher triaxiality. The stress state is therefore more complicated than that of the full ring.

4.4. Effect of thin layer of aged specimen

As numerical modeling is available, this last section attempts to quantify the effect of an oxidized HDPE thin layer in the inner wall of the full ring. To this end, the layer thickness is taken to be 200 μm, following Devilliers et al. [1]. Its behavior is supposed to be stiffer than the virgin material. This layer was provided with material properties detailed in Table 6 corresponding to "Oxidized HDPE", obtained from model aged material [1].

Figure 14a compares, the engineering stress–strain curves from the full ring test at 100 mm/mn, in terms of experimental, 3D FE simulation for virgin HDPE, 2D simulation with plane strain conditions with virgin HDPE and 2D simulation with 200 μm layer of oxidized HDPE. Simulations in 2D

Fig. 13. Notched ring: 3D representation of the stresses distribution in the net section at maximum stress $\sigma_{net}^{max} = 27$ MPa for 100 mm/mn crosshead speed. a) normalized hoop stress $\sigma_{yy}/\sigma_{net}^{max}$; b) normalized longitudinal stress $\sigma_{zz}/\sigma_{net}^{max}$; c) normalized radial stress $\sigma_{xx}/\sigma_{net}^{max}$.

plane strain are "stiffer" than 3D and experimental. This classical result is essentially due to 2D plane strain being applicable in the plane at half thickness. Comparison between oxidized and virgin tube focuses only on these 2D plane strain results. Namely, it can be observed that the increase of stress due to the oxidized layer is within the scatter band observed experimentally. One can conclude that the stress–strain curve is not sensitive to such a fraction of oxidized layer.

Concerning the local stresses, Fig. 14b displays the normalized stress distributions in the thickness, where symbols stand for full HDPE stresses and lines for HDPE with oxidized layer. The main feature is the discontinuity in the stress at the interface oxidized/
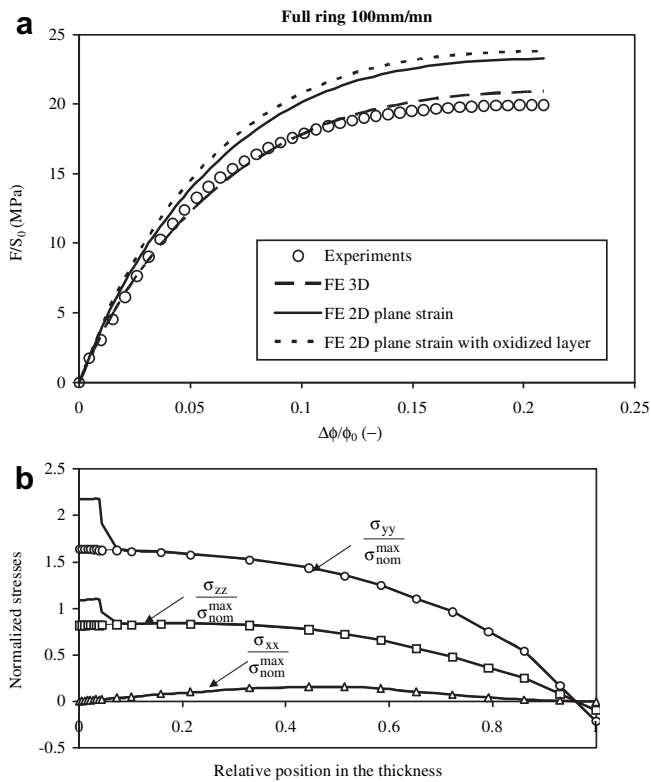
Fig. 14. Curves comparing full ring with/without 200 μm layer of oxidized material, at maximum stress $\sigma_{nom}^{max} = 20$ MPa for 100 mm/mn crosshead speed. a) stress–strain curves; b) normalized stresses.

virgin HDPE. The oxidized layer experiences higher stresses σ_{yy} and σ_{zz}, due to its mechanical response. Note that σ_{xx} is not affected by this overstress and its value remains negligible even under plane strain conditions. Furthermore, it can be expected that this thin layer could be crushed by the half cylinder. In conclusion, care must be taken to interpret Nol ring test results to measure the degree of aging of the HDPE material.

5. Conclusions

The main purpose of Nol ring tests was to measure the transverse properties of structural tubing from which one cannot extract classical uniaxial tensile specimens. However, the measured engineering stress and strain are not representative of the true mechanical behavior of the material. Stress–strain curves were examined on either full rings or notched rings as proposed by the standard. Fixing the half disks and preventing their rotation, reduces differential necking events in the tested ring. Typically, full rings are easy to produce, easy to test and easy to model (2D modeling is sufficient). However, there are bending effects in the cross section and high values of strain at failure. By contrast, notched rings have a complex stress state and can be modeled only in 3D, which is time consuming. Nevertheless, the bending effect is reduced and the strain to failure is reduced by a factor of 10 compared with full ring results.

The HDPE under study exhibited non-linearities in term of deformation and strain rate effects. Using FE analysis, it was possible to derive constitutive models and determine relevant

material parameters by an inverse method optimization. The approach consists in adjusting the material parameters to obtain simulated global stress–strain curves (up to maximum stress) close to experimental ones. With an optimized set of material parameters, the local stress and strain tensors in the cross section perpendicular to the tensile direction were obtained. For full rings, the hoop stress is not homogeneous (presence of bending stress) and the stress state is biaxial in the prescribed cross section. For notched rings, the stress state is triaxial although the bending effect is reduced.

In terms of pipe degradation assessment, it was demonstrated that the strain at failure from Nol ring tests was not an appropriate parameter, due to uncertainties relative to the experimental setup itself. Moreover, FE simulations of virgin/oxidized full ring tests showed that a 200 μm oxidized layer in the inner wall of the ring (degraded pipe) does not change the engineering stress–strain curve. Therefore, the use of Nol ring tests to assess the degree of pipe degradation was clearly shown to be inappropriate.

References

[1] Devillers C, Laiarinandrasana L, Fayolle B, Gaudichet-Maurin E, Oberti S. Impact of chlorine dioxide on the microstructure of polyethylene pipes: study of a crack network. In: Proceedings of 14th international conference on deformation, yield and fracture of polymers, April 5–9, 2009, Rolduc Abbey, Kerkrade, the Netherlands.
[2] Rozental-Evesque M, Rabaud B, Sanchez M, Louis S and Bruzek C-E. The Nol Ring test: an improved tool for characterizing the mechanical degradation of non-failed polyethylene pipes house connections. In: Proceedings of Plastic Pipes Congress 2008, September 22–24, Budapest, Hungary.
[3] Metallic Materials-Tube-Ring Expanding Test, International Standard ISO 8495-8496.
[4] Bagci C. A new unified strength of materials solution for stresses in curved beams and rings. Journal of Mechanical Design 1992;114:231.
[5] Bagci C. Exact elasticity solutions for stresses and deflections in curved beam and rings of exponential and T-sections. Transactions of the ASME 1993;115:346.
[6] Arsène S, Bai J. A new approach to measuring transverse properties of structural tubing by a ring test. Journal of Testing and Evaluation, JTEVA 1996;24 (6):386.
[7] Arsène S, Bai J. A new approach to measuring transverse properties of structural tubing by a ring test–experimental investigation. Journal of Testing and Evaluation, JTEVA 1998;26(1):26.
[8] Standard test method for apparent hoop tensile strength of plastic or reinforced plastic pipe by split disk method. ASTM D 2290-04.
[9] Brandrup J, Immergut EH, editors. Polymer Handbook. 4th ed. Wiley Interscience; 1999.
[10] Davis GT, Eby RK. Glass transition of polyethylene: volume relaxation. Journal of Applied Physics 1973;44:4274.
[11] Chang SS. Thermal relaxation and glass transition in polyethylene. Journal of Polymer Science: Polymer Symposia 1973;43(1):43.
[12] Illers KH, Kolloid-Zeitschrift and Zeitschrift fur polymere 1963; 190:16; *ibid.* 1969; 231: 622; *ibid.* 1973; 251: 394; *ibid.* 1974; 252:1.
[13] Stehling FC, Mandelkern L. The glass temperature of linear polyethylene. Macromolecules 1970;3(2):242.
[14] Hendra PJ, Jobic HP, Holland-Moritz K. Low temperature crystallization in polyethylene and the value of Tg. Journal of Polymer Science: Polymer Letters Edition 1975;13:365.
[15] Bridgman PW. The stress distribution at the neck of a tension specimen. Transactions ASM 1944;32:553.
[16] Besson J, Foerch R. Large scale object-oriented finite element code design. Computer Methods in Applied Mechanics and Engineering 1997;142:165.
[17] Besson J, Le Riche R, Foerch R, Cailletaud G. Object oriented programming applied to the finite element Method–Part II: Application to Material Behavior. European Journal of Finite Elements (Revue Européenne des Eléments Finis), P. Breitkopf Ed., Hermes Publ. 1998;7(5):567.
[18] Ben Hadj Hamouda H, Laiarinandrasana L, Piques R. Viscoplastic behavior of a medium density polyethylene (MDPE): constitutive equations based on double nonlinear deformation model. International Journal of Plasticity 2007;23:1307.
[19] Regrain C, Laiarinandrasana L, Toillon S, Saï K. Multi-mechanism models for semi-crystalline polymers: constitutive equations and finite element implementation. International Journal of Plasticity 2009;25:1253.